Journal of Fluorine Chemistry 153 (2013) 61–67

Contents lists available at SciVerse ScienceDirect

Journal of Fluorine Chemistry

journal homepage: www.elsevier.com/locate/fluor

Colloidal lanthanide-doped $NaLuF_4:Ln^{3+}$ nanocrystals: Synthesis, energy transfer, and tunable luminescence properties

Shuai Liu [a], Guofeng Wang [a,*], Kai Pan [a], Ying Li [a], Li Feng [a], Chungui Tian [a], Baojiang Jiang [a], Naiying Fan [a], Qingmao Feng [a], Jisen Zhang [b,*]

[a] Key Laboratory of Functional Inorganic Material Chemistry, Ministry of Education, School of Chemistry and Materials Science, Heilongjiang University, Harbin 150080, China
[b] Changchun Institute of Optics, Fine Mechanics and Physics, Chinese Academy of Sciences, Changchun 130033, China

ARTICLE INFO

Article history:
Received 8 April 2013
Received in revised form 8 May 2013
Accepted 12 May 2013
Available online 24 May 2013

Keywords:
$NaLuF_4$
Lanthanide ions
Nanocrystals
Optical properties
Decay dynamics

ABSTRACT

Colloidal $NaLuF_4:Ln^{3+}$ (Ln = Yb/Er, Yb/Gd/Tm, and Gd/Eu) nanocrystals were synthesized by a hydrothermal method. The effects of $NaF/Ln(NO_3)_3$ ratio on the phase compositions, morphologies, and luminescence properties of $NaLuF_4:Ln^{3+}$ nanocrystals were investigated in detail. The results indicated that larger $NaF/Ln(NO_3)_3$ ratio is benefit for the formation of hexagonal phase $NaLuF_4:Ln^{3+}$. Multicolor up-conversion luminescence tuning of $NaLuF_4:Ln^{3+}$ nanocrystals was successfully achieved by adjusting lanthanide-ion-doped content. Especially, the $^6P_{7/2} \rightarrow {}^8S_{7/2}$ (~313 nm) transition from Gd^{3+} ions was observed in $NaLuF_4:Yb^{3+}/Gd^{3+}/Tm^{3+}$ nanorods under 980 nm excitation. Decay dynamics was performed to study the down-conversion luminescence properties of the $NaLuF_4:Gd^{3+}/Eu^{3+}$ nanorods. All the decay curves can be well fitted with a second order exponential decay function.

1. Introduction

Inorganic compounds doped with lanthanide ions have attracted much attention due to their potential applications in many areas of material science [1–9]. Compared with conventional luminescent materials, such as organic fluorescent dyes and semiconductor quantum dots, lanthanide-doped materials have narrow emission bands, low photobleaching, and longer luminescent lifetimes [10,11]. Furthermore, by tuning different lanthanide-ion-doped content, these phosphors can emit multicolor down- and up-converting luminescence [12–14].

In recent years, the controllable synthesis of nanocrystals has attracted considerable interest driven primarily by the fact that the shape and size of nanocrystals have tremendous effects on their properties [15,16]. Especially, much effort has been devoted to the synthesis of micro/nanocrystals doped with lanthanide ions, since Bhargava et al. reported that $ZnS:Mn^{2+}$ nanocrystals yielded high luminescence efficiencies [17].

Among various nanomaterials, fluoride nanocrystals have attracted considerable attention, because lanthanide doped fluorides have low phonon energies and high quantum efficiencies as luminescent materials [18–20]. In particular, hexagonal phase $NaYF_4$ is acknowledged as the most efficient down- and up-conversion host materials for a long time [21,22]. Recently, Qin et al. have found that hexagonal phase $NaLuF_4$ is a more attractive host for phosphors with interesting up-conversion luminescent properties [23,24]. However, few systematic studies on size-dependent luminescent behavior of $NaLuF_4:Ln^{3+}$ nanocrystals were reported. Especially, decay dynamics in $NaLuF_4:Gd^{3+}/Eu^{3+}$ nanorods has received little attention. In addition, Gd^{3+} is an ideal paramagnetic relaxation agent used in magnetic resonance imaging because of its large magnetic moment and nanosecond time scale electronic relaxation time [25]. Therefore, the Gd^{3+} doped systems are very attractive to produce single-phase multifunctional nanocrystals, such as paramagnetism and multicolor luminescence.

Herein, we have successfully synthesized $NaLuF_4:Ln^{3+}$ (Ln = Yb/Er, Yb/Gd/Tm, and Gd/Eu) nanocrystals by using a hydrothermal method. It was found that larger $NaF/Ln(NO_3)_3$ ratio is benefit for the formation of hexagonal phase $NaLuF_4:Ln^{3+}$. The luminescent properties of samples were studied systemically. Multicolor up-conversion luminescence tuning of $NaLuF_4:Ln^{3+}$ nanocrystals was successfully achieved. Decay dynamics was performed to study the down-conversion luminescence of the $NaLuF_4:Gd^{3+}/Eu^{3+}$ nanorods.

* Corresponding authors. Tel.: +86 451 89359680; fax: +86 451 89359680.
E-mail addresses: wanggf75@gmail.com (G. Wang), zhangjisen1962@163.com (J. Zhang).

0022-1139/$ – see front matter © 2013 Elsevier B.V. All rights reserved.
http://dx.doi.org/10.1016/j.jfluchem.2013.05.018

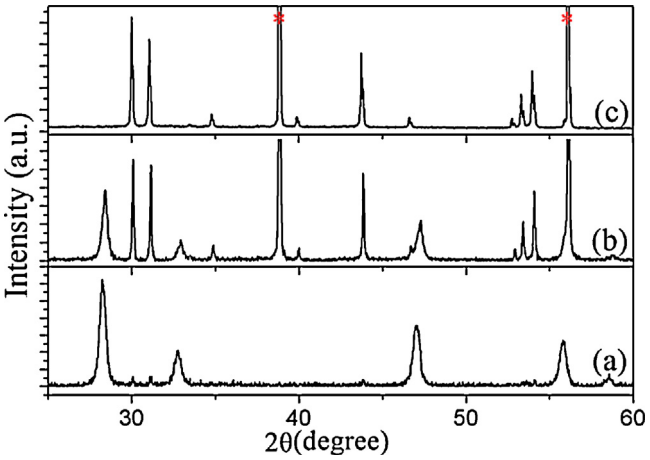

Fig. 1. XRD patterns of $NaLuF_4$:Yb^{3+}(20%)/Er^{3+}(0.5%) nanocrystals prepared with the $NaF/Ln(NO_3)_3$ ratio of (a) 6, (b) 12, and (c) 32, respectively.

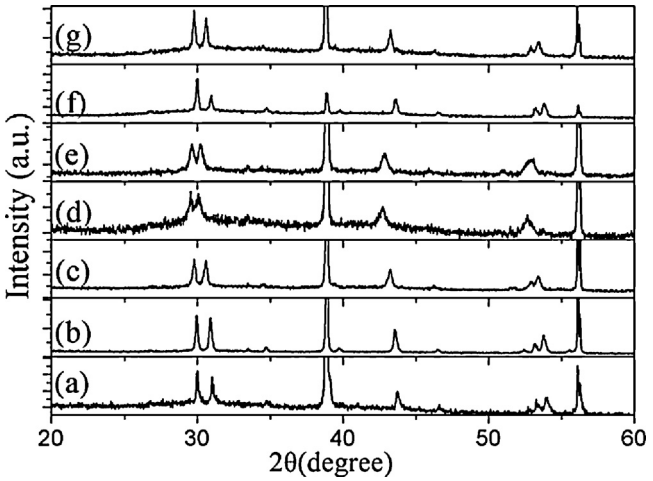

Fig. 2. XRD patterns of (a) $NaLuF_4$:Eu^{3+}(10%), (b) $NaLuF_4$:Gd^{3+}(15%)/Eu^{3+}(10%), (c) $NaLuF_4$:Gd^{3+}(30%)/Eu^{3+}(10%), (d) $NaLuF_4$:Gd^{3+}(60%)/Eu^{3+}(10%), (e) $NaLuF_4$:Gd^{3+}(80%)/Eu^{3+}(10%), (f) $NaLuF_4$:Gd^{3+}(20%)/Eu^{3+}(15%), and (g) $NaLuF_4$:Gd^{3+}(20%)/Eu^{3+}(50%) prepared at 180 °C for 24 h.

2. Results and discussion

2.1. Crystal structure and morphology

The crystal structures and particle sizes of products were obtained by X-ray diffraction (XRD) patterns. Fig. 1 shows the XRD patterns of $NaLuF_4$:Yb^{3+}/Er^{3+} nanocrystals prepared at 180 °C for 24 h. When the $NaF/Ln(NO_3)_3$ ratios were 6 and 12, hexagonal and cubic phase $NaLuF_4$:Yb^{3+}/Er^{3+} nanocrystals coexisted. When the $NaF/Ln(NO_3)_3$ ratio was 32, pure hexagonal phase $NaLuF_4$:Yb^{3+}/Er^{3+} nanorods were obtained. The results indicated that larger $NaF/Ln(NO_3)_3$ ratio was benefit for the formation of hexagonal phase $NaLuF_4$. The peaks marked by asterisk (*) arise from excessive cubic NaF. The XRD patterns of the hexagonal phase $NaLuF_4$:Gd^{3+}/Eu^{3+} ($NaF/Ln(NO_3)_3$ = 32) with different Gd^{3+}/Eu^{3+} concentrations are shown in Fig. 2. In addition, from the bottom to top in Fig. 2(a)–(e), the XRD patterns become broader and broader, suggesting that the crystalline size gradually decreased with increasing Gd^{3+} concentration.

The size and morphology of the final products were investigated by transmission electron microscope (TEM). Fig. 3(a) shows the TEM image of $NaLuF_4$:Yb^{3+}(20%)/Er^{3+}(0.5%) nanocrystals prepared with the $NaF/Ln(NO_3)_3$ ratio of 6, which is a sphere-like structure with a mean diameter of ~20 nm. The high-resolution transmission electron microscopy (HRTEM) image of a single nanoparticle is shown in Fig. 3(b). The measured lattice spacing is about 0.311 nm, corresponding to the distance of the {1 1 1} planes of the cubic $NaLuF_4$:Yb^{3+}/Er^{3+}. This image also reveals the single-crystal nature of the product. Fig. 3(c) shows the TEM image of $NaLuF_4$:Eu^{3+}(10%) nanocrystals prepared with the $NaF/Ln(NO_3)_3$ ratio of 32. The nanorods are ~50 nm in diameter and ~400 nm in length. Fig. 3(d) shows the HRTEM image of a single nanorod. The measured lattice spacing is about 0.193 nm, corresponding to the distance of the {2 1 0} planes of the hexagonal phase $NaLuF_4$:Eu^{3+}(10%). Fig. 3(e) and (f) shows the TEM images of $NaLuF_4$:Gd^{3+}(20%)/Eu^{3+}(10%) nanocrystals prepared with the $NaF/Ln(NO_3)_3$ ratio of 32. The

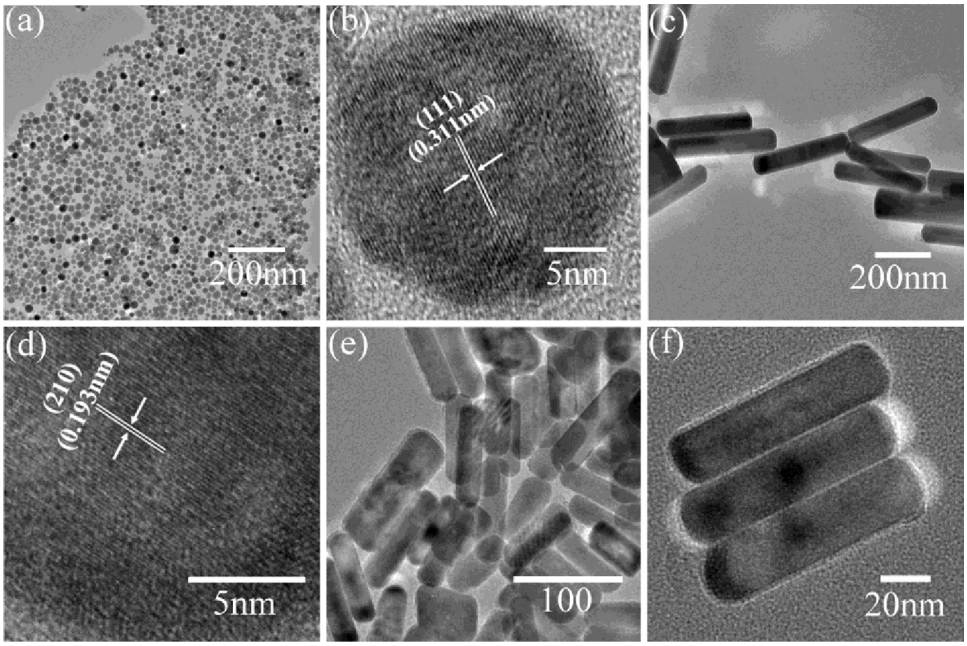

Fig. 3. TEM and HRTEM images of (a, b) $NaLuF_4$:Yb^{3+}(20%)/Er^{3+}(0.5%) ($NaF/Ln(NO_3)_3$ = 6), (c, d) $NaLuF_4$:Eu^{3+}(10%) ($NaF/Ln(NO_3)_3$ = 32), and (e, f) $NaLuF_4$:Gd^{3+}(30%)/Eu^{3+}(10%) ($NaF/Ln(NO_3)_3$ = 32).

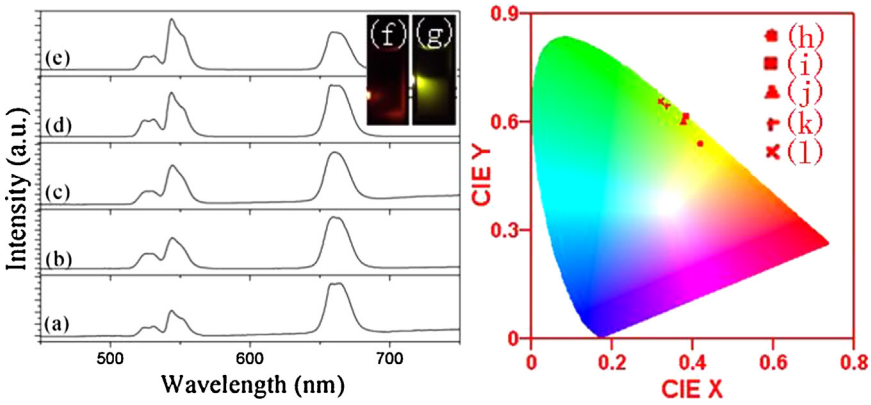

Fig. 4. Up-conversion luminescence spectra and corresponding CIE 1931 chromaticity diagram of $NaLuF_4$:Yb^{3+}(20%)/Er^{3+}(0.5%) nanocrystals prepared with the NaF/$Ln(NO_3)_3$ ratio of (a, h) 6, (b, i) 8, (c, j) 12, (d, k) 24, and (e, l) 32, respectively. Inset shows the luminescent photos of $NaLuF_4$:Gd^{3+}(20%)/Yb^{3+}(20%)/Tm^{3+}(0.5%) nanocrystals prepared with the NaF/$Ln(NO_3)_3$ ratio of (f) 6 and (g) 32 dissolved in cyclohexane under 980 nm excitation (without the use of a filter).

Table 1
The CIE chromaticity coordinates calculated from the up-conversion luminescence spectra of $NaLuF_4$:Yb^{3+}(20%)/Er^{3+}(0.5%) nanocrystals prepared with different NaF/$Ln(NO_3)_3$ ratio.

NaF/$Ln(NO_3)_3$ ratio	6	8	12	24	32
CIE (x, y) of Er^{3+}	(0.419, 0.542)	(0.384, 0.614)	(0.375, 0.601)	(0.335, 0.645)	(0.32, 0.658)

nanorods are ~20 nm in diameter and ~80 nm in length. Obviously, the mean size of nanorods decreased with increasing Gd^{3+} concentration.

2.2. Luminescence properties

Fig. 4 shows the up-conversion luminescence spectra of the $NaLuF_4$:Yb^{3+}(20%)/Er^{3+}(0.5%) nanocrystals prepared with different NaF/$Ln(NO_3)_3$ ratio under 980 nm excitation. The emission peaks can be attributed to the $^2H_{11/2} \rightarrow {}^4I_{15/2}$, $^4S_{3/2} \rightarrow {}^4I_{15/2}$, and $^4F_{9/2} \rightarrow {}^4I_{15/2}$ transitions of Er^{3+} ions. Obviously, the relative intensity of $^2H_{11/2}/{}^4S_{3/2} \rightarrow {}^4I_{15/2}$ to $^4F_{9/2} \rightarrow {}^4I_{15/2}$ rises with increasing the NaF/$Ln(NO_3)_3$ ratio, which will be discussed later. The CIE chromaticity coordinates were calculated from the up-conversion luminescence spectra, as shown in Table 1. The CIE coordinates of the up-conversion luminescence were (0.419, 0.542), (0.384, 0.614), (0.375, 0.601), (0.335, 0.645), and (0.32, 0.658) for the NaF/$Ln(NO_3)_3$ ratio of 6, 8, 12, 24, and 32, respectively. Obviously, the CIE coordinates changed with the NaF/$Ln(NO_3)_3$ ratio.

Fig. 5 shows the double logarithmic plots of the emission intensity as a function of excitation power for the $^2H_{11/2}/{}^4S_{3/2} \rightarrow {}^4I_{15/2}$ and $^4F_{9/2} \rightarrow {}^4I_{15/2}$ emissions in $NaLuF_4$:Yb^{3+}/Er^{3+} nanocrystals prepared with different NaF/$Ln(NO_3)_3$ ratio. Theoretically, the emission intensity is proportional to the n-th power of the excitation intensity, and the integer n is the number of photons absorbed per up-converted photon emitted [26]. For the red emission, the values of n were determined to be 1.70 and 1.81 in the $NaLuF_4$:Yb^{3+}/Er^{3+} nanocrystals prepared with the NaF/$Ln(NO_3)_3$ ratio of 6 and 32, respectively. For the green emissions, the values of n were determined to be 1.98 and 2.27 in the $NaLuF_4$:Yb^{3+}/Er^{3+} nanocrystals prepared with the NaF/$Ln(NO_3)_3$ ratio of 6 and 32, respectively. Obviously, the values of n increased with decreasing the size of nanocrystals, and the slopes of the red emission are smaller than those of the green emissions. A larger value than 2 suggests that a three-photon process should be involved for populating the green levels. Many results indicated that the three-photon process was dominant for populating the green-emitting level $^4S_{3/2}/{}^2H_{11/2}$ as the Yb^{3+} concentration was high enough. The present result indicates that the smaller the

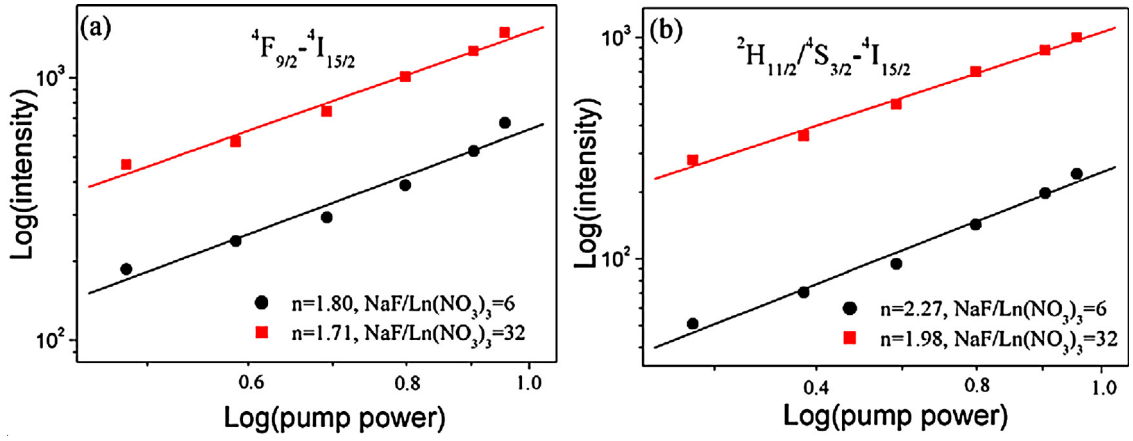

Fig. 5. Plots (log–log) of emission intensity versus excitation power in $NaLuF_4$:Yb^{3+}(20%)/Er^{3+}(0.5%) prepared with different NaF/$Ln(NO_3)_3$ ratio.

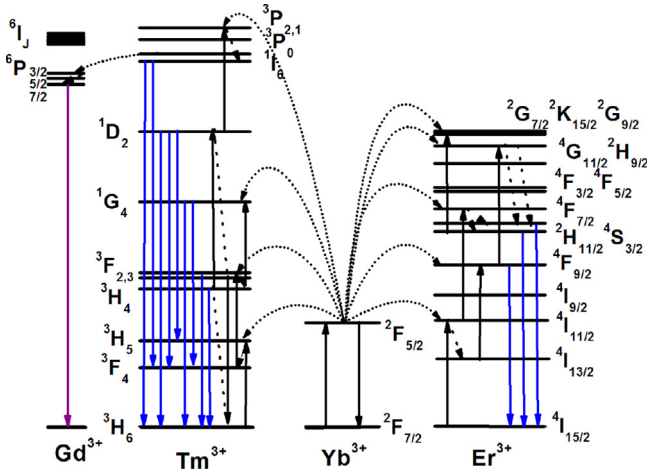

Fig. 6. Energy-level and up-conversion schemes for the Yb^{3+}–Tm^{3+}–Gd^{3+} and Yb^{3+}–Er^{3+} systems.

particle size is, the easier the three-photon process for the green is. The processes of infrared excitation and up-conversion emissions were drawn in the energy level diagrams of Yb^{3+} and Er^{3+} ions, as shown in Fig. 6.

We suggest that the variation of the relative intensity of $^4F_{9/2} \rightarrow {}^4I_{15/2}$ to $^2H_{11/2}/{}^4S_{3/2} \rightarrow {}^4I_{15/2}$ is correlated with the oxygen impurities, surface ligands, and surface defect of the $NaLuF_4$:Yb^{3+}/Er^{3+} nanocrystals [27]. It is noted that the nonradiative decay of the $NaLuF_4$:Yb^{3+}/Er^{3+} nanocrystals might be partially correlated with the influence between the surface defect, ligands, and surface Er^{3+} ions. As the ratio of the surface defects decreases with increasing size of the nanocrystals, the nonradiative relaxation of the $^4I_{11/2}$ to $^4I_{13/2}$ level in the Er^{3+} ion is decreased. Therefore, the red $^4F_{9/2} \rightarrow {}^4I_{15/2}$ emission as well as the relative intensity of $^4F_{9/2} \rightarrow {}^4I_{15/2}$ to $^2H_{11/2}/{}^4S_{3/2} \rightarrow {}^4I_{15/2}$ decreased with increasing the size of nanocrystals.

Fig. 7 shows the up-conversion luminescence spectrum of the as-prepared $NaLuF_4$:Gd^{3+}/Yb^{3+}/Tm^{3+} nanocrystals under 980 nm excitation. The emission peaks can be attributed to the $^1I_6 \rightarrow {}^3H_6$, $^1I_6 \rightarrow {}^3F_4$, $^1D_2 \rightarrow {}^3H_6$, $^1D_2 \rightarrow {}^3F_4$, $^1G_4 \rightarrow {}^3H_6$, $^1D_2 \rightarrow {}^3H_5$, $^1G_4 \rightarrow {}^3F_4$, and $^3F_3 \rightarrow {}^3H_6$ transitions. It is obvious that the $^6P_{7/2} \rightarrow {}^8S_{7/2}$ transition of Gd^{3+} ions was observed, indicating the energy transfer

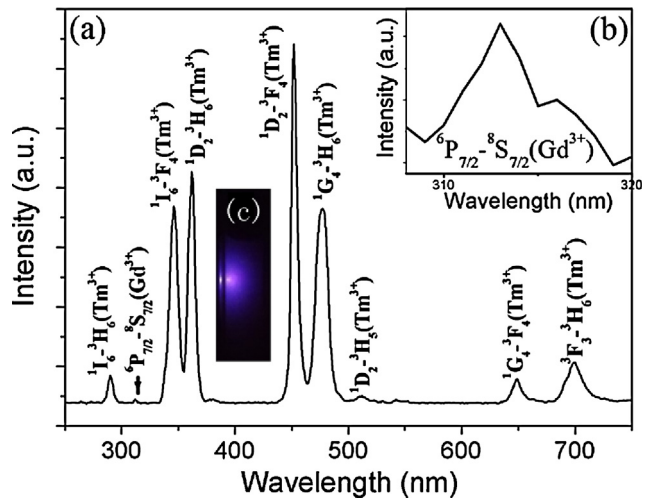

Fig. 7. (a) Up-conversion luminescence spectrum of $NaLuF_4$:Gd^{3+}(20%)/Yb^{3+}(20%)/Tm^{3+}(0.5%) nanocrystals prepared with the NaF/$Ln(NO_3)_3$ ratio of 32. (b) Magnification of the spectrum in the range of 308–320 nm. (c) The luminescence photograph of $NaLuF_4$:Gd^{3+}(20%)/Yb^{3+}(20%)/Tm^{3+}(0.5%) nanocrystals dissolved in cyclohexane under 980 nm excitation (without the use of a filter).

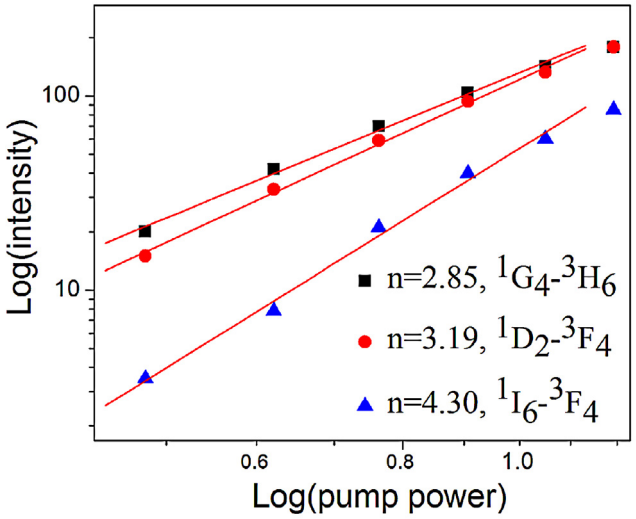

Fig. 8. Plots (log–log) of emission intensity versus excitation power in $NaLuF_4$:Gd^{3+}(20%)/Yb^{3+}(20%)/Tm^{3+}(0.5%) nanocrystals prepared with the NaF/$Ln(NO_3)_3$ ratio of 32.

from Yb^{3+} to Tm^{3+}, then to Gd^{3+} ions. In addition, the dominant emission is the $^1D_2 \rightarrow {}^3F_4$ transition. The naked-eye-visible blue up-conversion luminescence photo of $NaLuF_4$:Gd^{3+}/Yb^{3+}/Tm^{3+} nanocrystals dissolved in cyclohexane was also depicted, as shown in Fig. 7(c).

Fig. 8 shows the double logarithmic plots of the emission intensity as a function of excitation power for the $^1I_6 \rightarrow {}^3F_4$, $^1D_2 \rightarrow {}^3F_4$, and $^1G_4 \rightarrow {}^3H_6$ emissions in $NaLuF_4$:Gd^{3+}/Yb^{3+}/Tm^{3+} nanocrystals. The values of n for the $^1I_6 \rightarrow {}^3F_4$, $^1D_2 \rightarrow {}^3F_4$, and $^1G_4 \rightarrow {}^3H_6$ emissions were determined to be 4.30, 3.19, and 2.85, respectively. The processes of infrared excitation and up-conversion emissions were drawn in the energy level diagrams of Tm^{3+}, Yb^{3+}, and Gd^{3+} ions, as shown in Fig. 6. The near infrared up-conversion luminescence occurs via a two-step energy transfer from Yb^{3+} to Tm^{3+}. First, the Tm^{3+} ions are excited from the ground state $^3H_6$ to the excited state $^3H_5$ via energy transfer of neighboring Yb^{3+} and Tm^{3+}. Subsequent nonradiative relaxation of $^3H_5 \rightarrow {}^3F_4$ populates the $^3F_4$ level. In the second-step excitation, the same laser pumps the excited-state ions from the $^3F_4$ to the $^3F_2$ state via energy transfer. The populated $^3F_2$ may nonradiatively relax to two levels: $^3F_3$ and $^3H_4$. The electrons in the $^3H_4$ level may be partly excited to the $^1G_4$ level via phonon-assisted energy transfer by the third photon. The $^1D_2$ level of Tm^{3+} cannot be populated by the fourth photon from Yb^{3+} to the $^1G_4$ level via energy transfer due to the large energy mismatch (about 3500 cm^{-1}) between them [28]. The cross relaxation process of $^3F_2 + {}^3H_4 \rightarrow {}^3H_6 + {}^1D_2$ between Tm^{3+} ions may alternatively play an important role in populating $^1D_2$ level [2,24]. The populated $^1D_2$ level relaxes radiatively to the ground-state and inter-states, which cause 364 and 453 nm emissions. On the other hand, the electron in the $^1D_2$ level may be excited to the $^1I_6$ level via another energy transfer process, produce 292 and 348 nm emissions, simultaneously. Finally, the $^6P_{7/2}$ level of Gd^{3+} was populated via another energy transfer from Tm^{3+} to Gd^{3+}.

Fig. 9 shows the room-temperature excitation spectra (monitored at 595 and 619 nm) of $NaLuF_4$:Gd^{3+}(20%)/Eu^{3+} with different Eu^{3+} concentrations. The excitation lines corresponds to the $^8S_{7/2} \rightarrow {}^6D_J$ and $^8S_{7/2} \rightarrow {}^6I_J$ transitions of Gd^{3+} ions and the $^7F_0 \rightarrow {}^5F_{2,4}$, $^7F_0 \rightarrow {}^5H_3$, $^7F_0 \rightarrow {}^5D_4$, $^7F_0 \rightarrow {}^5L_7$, and $^7F_0 \rightarrow {}^5L_6$ transitions of Eu^{3+} ions. The most intense peak is centered at 393 nm. The relative intensity of the transitions from Gd^{3+} to those from Eu^{3+} decreases with increasing Eu^{3+} concentrations. The charge-transfer

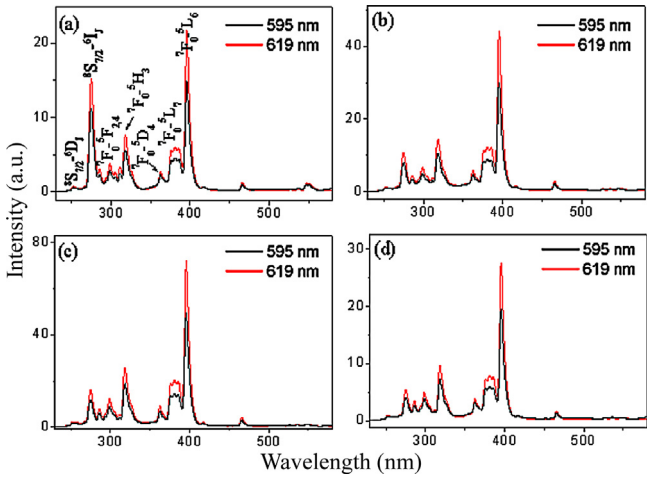

Fig. 9. Excitation spectra of (a) $NaLuF_4:Gd^{3+}(20\%)/Eu^{3+}(15\%)$, (b) $NaLuF_4:Gd^{3+}(20\%)/Eu^{3+}(30\%)$, (c) $NaLuF_4:Gd^{3+}(20\%)/Eu^{3+}(40\%)$, and (d) $NaLuF_4:Gd^{3+}(20\%)/Eu^{3+}(50\%)$ monitored at different emission wavelengths.

transition of pure fluoride systems usually exists in the vacuum ultraviolet region as a result of high electronegativity. Under current experimental condition, we cannot further explore the ultraviolet-excited fluorescence in the $NaLuF_4:Gd^{3+}(20\%)/Eu^{3+}$ nanocrystals.

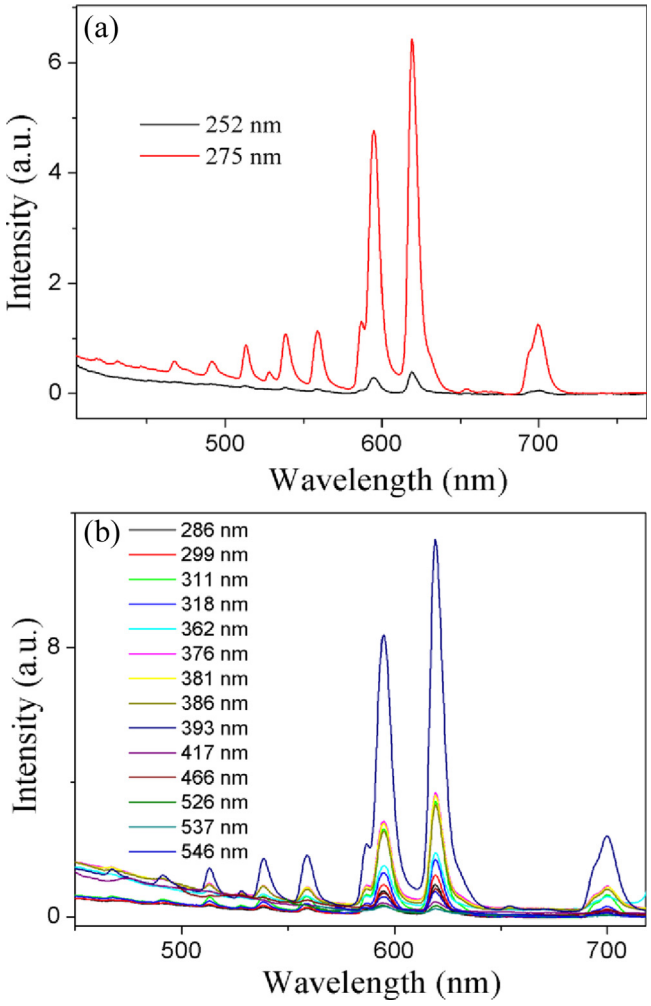

Fig. 10. Emission spectra of $NaLuF_4:Gd^{3+}(20\%)/Eu^{3+}(15\%)$ excited at different wavelengths.

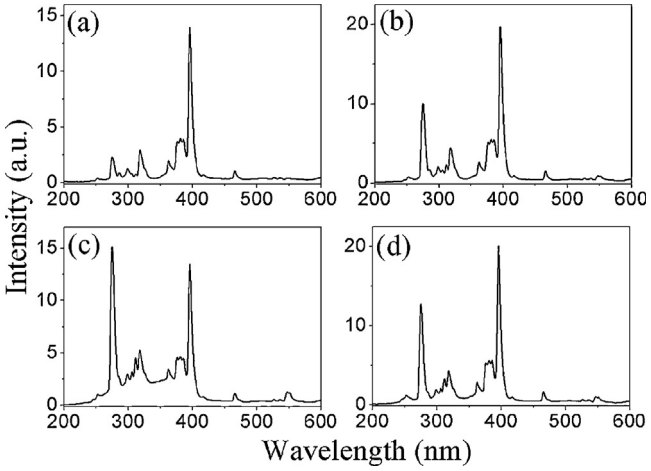

Fig. 11. Excitation spectra of (a) $NaLuF_4:Gd^{3+}(15\%)/Eu^{3+}(10\%)$, (b) $NaLuF_4:Gd^{3+}(30\%)/Eu^{3+}(10\%)$, (c) $NaLuF_4:Gd^{3+}(60\%)/Eu^{3+}(10\%)$, and (d) $NaLuF_4:Gd^{3+}(80\%)/Eu^{3+}(10\%)$ monitored at 619 nm.

Fig. 10(a) shows the emission spectra of $NaLuF_4:Gd^{3+}(20\%)/Eu^{3+}(15\%)$ under 252 and 275 nm excitation, which corresponds to the $^8S_{7/2} \rightarrow {}^6D_J$ and $^8S_{7/2} \rightarrow {}^6I_J$ transitions of Gd^{3+} ions, respectively. The $^5D_2 \rightarrow {}^7F_0$ (~467 nm), $^5D_2 \rightarrow {}^7F_2$ (~492 nm), $^5D_2 \rightarrow {}^7F_3$ (514 nm), $^5D_1 \rightarrow {}^7F_0$ (~528 nm), $^5D_1 \rightarrow {}^7F_1$ (~538 nm), $^5D_1 \rightarrow {}^7F_2$ (~559 nm), $^5D_1 \rightarrow {}^7F_3$ (~587 nm), $^5D_0 \rightarrow {}^7F_1$ (~595 nm), $^5D_0 \rightarrow {}^7F_2$ (~619 nm), $^5D_0 \rightarrow {}^7F_3$ (~654 nm), and $^5D_0 \rightarrow {}^7F_4$ (~700 nm) transitions of Eu^{3+} ions were observed. These results further confirm that effective energy transfer could occur from Gd^{3+} to Eu^{3+}. In addition, the luminescence was dominated by $^5D_0 \rightarrow {}^7F_2$ transition. Fig. 10(b) shows the emission spectra of $NaLuF_4:Gd^{3+}(20\%)/Eu^{3+}(15\%)$ excited at different wavelengths, which corresponds to the transitions of Eu^{3+} ions. The peak positions and spectral shapes of emissions were independent of excitation wavelengths.

Fig. 11 shows the excitation spectra (monitored at 619 nm) of $NaLuF_4:Gd^{3+}/Eu^{3+}(10\%)$ with different Gd^{3+} concentrations. The relative intensity of the transition of Gd^{3+} ions to those of Eu^{3+} ions increases with increasing Gd^{3+} concentrations, up to about 60 mol%, and then decreased abruptly. Fig. 12 shows the emission spectra of $NaLuF_4:Gd^{3+}/Eu^{3+}(10\%)$ with different Gd^{3+} concentrations under 393 nm excitation.

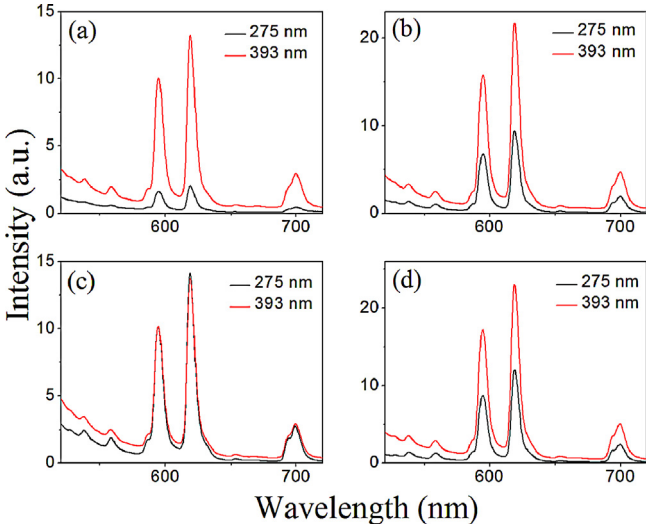

Fig. 12. Emission spectra of (a) $NaLuF_4:Gd^{3+}(15\%)/Eu^{3+}(10\%)$, (b) $NaLuF_4:Gd^{3+}(30\%)/Eu^{3+}(10\%)$, (c) $NaLuF_4:Gd^{3+}(60\%)/Eu^{3+}(10\%)$, and (d) $NaLuF_4:Gd^{3+}(80\%)/Eu^{3+}(10\%)$ excited at different wavelengths.

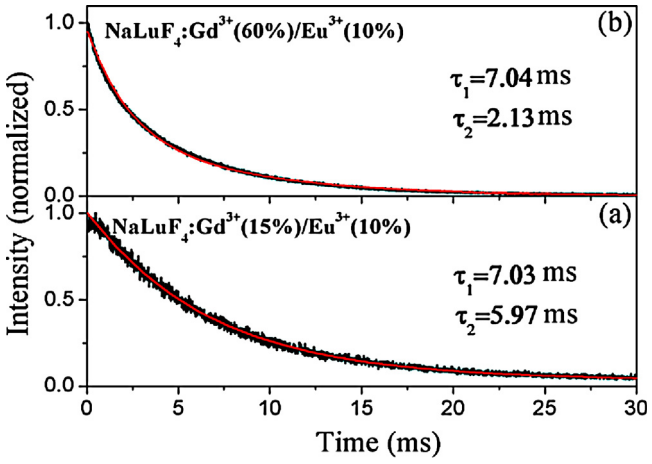

Fig. 13. Luminescence decay curves for the $NaLuF_4:Gd^{3+}/Eu^{3+}$ nanorods excited at 355 nm and monitored at 619 nm.

Fig. 13 shows the luminescence decay traces of the $NaLuF_4:Gd^{3+}/Eu^{3+}$(10%) with different Gd^{3+} concentrations by monitoring the peak emission at 619 nm. All the decay curves can be well fitted with a second order exponential decay function. Two components are determined from the fitting and the corresponding values for each curve are listed in Fig. 13: $\tau_1 = 7.03$ and $\tau_2 = 5.97$ for $NaLuF_4:Gd^{3+}$(15%)/Eu^{3+}(10%); $\tau_1 = 7.04$ and $\tau_2 = 2.13$ for $NaLuF_4:Gd^{3+}$(60%)/Eu^{3+}(10%). It is well known that the lifetime τ is determined by the radiative transition rate (W_{rad}) and the nonradiative transition rate (W_{nr}), which can be written as [29]

$$\tau = \frac{1}{W_{rad} + W_{nr}} \quad (1)$$

The nonradiative relaxation rate increased dramatically with decreasing particle size due to a great number of surface defects. We suggested that the longer lifetimes (τ_1) correspond to the $^5D_0$ level of the Eu^{3+} ions inside nanorods, was almost independent of Gd^{3+} concentrations. However, the value of τ_2 for $NaLuF_4:Gd^{3+}$(60%)/Eu^{3+}(10%) is much shorter than that for $NaLuF_4:Gd^{3+}$(15%)/Eu^{3+}(10%), which can be attributed to the decrease of the size of nanorods. And thus, τ_2 should correspond to the $^5D_0$ level of the Eu^{3+} ions near the surface.

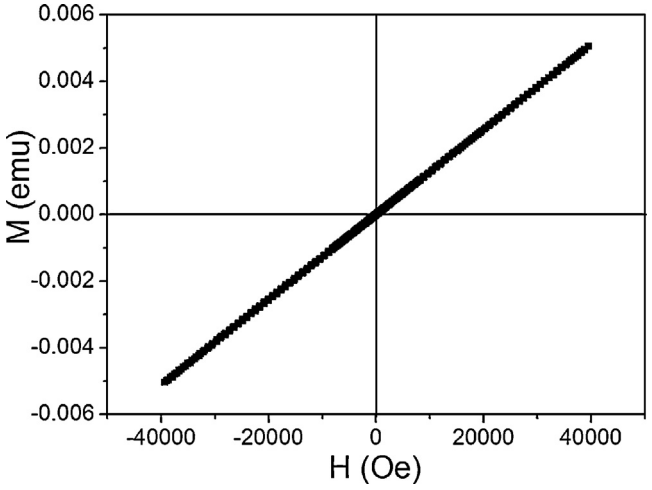

Fig. 14. Magnetization curve of $NaLuF_4:Gd^{3+}$(60%)/Eu^{3+}(10%) nanorods at room temperature.

In addition to the aforementioned luminescence properties, these Gd^{3+} doped $NaLuF_4$ nanocrystals also present paramagnetic properties, as shown in Fig. 14. These UC luminescent and paramagnetic properties of the nanorods underscore their potential as robust UC luminescence and magnetic resonance dual-mode fluorescent labels for bioimaging applications.

3. Conclusion

$NaLuF_4:Ln^{3+}$ (Ln = Yb/Er, Yb/Gd/Tm, and Gd/Eu) nanocrystals were synthesized by a hydrothermal method. The effects of NaF/$Ln(NO_3)_3$ ratio on the phase compositions, morphologies, and luminescence properties of $NaLuF_4:Ln^{3+}$ nanocrystals were investigated in detail. The results indicated that larger NaF/$Ln(NO_3)_3$ ratio is benefit for the formation of hexagonal phase $NaLuF_4:Ln^{3+}$. Multicolor up-conversion luminescence tuning of $NaLuF_4:Ln^{3+}$ nanocrystals was successfully achieved by adjusting lanthanide-ion-doped content. In the up-conversion luminescence spectra of $NaLuF_4:Yb^{3+}/Er^{3+}$ nanorods, the relative intensity of $^2H_{11/2}/^4S_{3/2} \rightarrow {}^4I_{15/2}$ to $^4F_{9/2} \rightarrow {}^4I_{15/2}$ rises with increasing the NaF/$Ln(NO_3)_3$ ratio. In addition, the $^6P_{7/2} \rightarrow {}^8S_{7/2}$ (~313 nm) transition from Gd^{3+} ions was observed in $NaLuF_4:Yb^{3+}/Gd^{3+}/Tm^{3+}$ nanorods under 980 nm excitation. Decay dynamics was performed to study the down-conversion luminescence properties of the $NaLuF_4:Gd^{3+}/Eu^{3+}$ nanorods. All the decay curves can be well fitted with a second order exponential decay function. The energy transfer between Gd^{3+} and Eu^{3+} was also investigated. In addition to the aforementioned luminescence properties, these Gd^{3+} tridoped nanorods also exhibit paramagnetic behavior at room temperature

4. Experimental

4.1. Synthesis

Synthesis of $NaLuF_4:Ln^{3+}$ nanocrystals: in a typical synthesis, 1 mL of $Ln(NO_3)_3$ aqueous solution (0.5 mol/L) and NaF aqueous solution were added to a mixture of NaOH (1.2 g), ethanol (8 mL), deionized water (4 mL), and oleic acid (20 mL), and the solution was thoroughly stirred. Subsequently, the milky colloidal solution was transferred to a 50 mL Teflon-lined autoclave, and heated at 180 °C for 24 h. The systems were then allowed to cool to room temperature. The final products were collected by means of centrifugation, washed with ethanol, and finally dried in vacuum at 80 °C.

4.2. Characterization

The crystal structure was analyzed by a Rigaku (Japan) D/MAX-rA X-ray diffractionmeter equipped with graphite monochromatized Cu Kα radiation (γ = 1.541874 Å), keeping the operating voltage and current at 40 kV and 40 mA, respectively. The size and morphology of the final products were determined by using JEOL JEM-2010F transmission electron microscope operated at 200 kV. The down-conversion luminescence spectra were recorded with a Hitachi F-4600 fluorescence spectrophotometer at room temperature. For comparison of the luminescence properties of different samples, the luminescence spectra were measured with the same instrument parameters (2.5 nm for slit width and 400 V for PMT voltage). The up-conversion luminescence spectra were recorded using the spectrophotometer with an adjustable laser (980 nm, Beijing Hi-Tech Optoelectronic Co., China) as the excitation source with a fiber-optic accessory. Luminescence decay curves were measured under the excitation of a third harmonic (355 nm) of a Nd:YAG pulsed laser.

Acknowledgements

This work was supported by the National Natural Science Foundation of China (21001042, 11174276, and 21171052), the Program for New Century Excellent Talents in University of Ministry of Education of China (NCET-11-0959), the Postdoctoral Science Foundation of Heilongjiang Province (LBH-Q11009), Harbin technological innovation talent of special funds (2013RFQXJ136), and the Youth Foundation for Distinguished Young Scholars of Heilongjiang University.

References

[1] X. Wang, J. Zhuang, Q. Peng, Y.D. Li, Nature 437 (2005) 121–124.
[2] G.F. Wang, W.P. Qin, L.L. Wang, G.D. Wei, P.F. Zhu, R. Kim, Opt. Express 16 (2008) 11907–11914.
[3] F. Williams, A.J. Nozik, Nature 312 (1984) 21–27.
[4] L.Y. Wang, R.X. Yan, Z.Y. Huo, L. Wang, J.H. Zeng, J. Bao, X. Wang, Q. Peng, Y.D. Li, Angew. Chem. 117 (2005) 6208–6211.
[5] C.X. Li, J. Yang, Z.W. Quan, P.P. Yang, D.Y. Kong, J. Lin, Chem. Mater. 19 (2007) 4933–4942.
[6] Y. Zhang, F. Zheng, T. Yang, W. Zhou, Y. Liu, N. Man, L. Zhang, N. Jin, Q. Dou, Y. Zhang, Z. Li, L. Wen, Nat. Mater. 11 (2012) 817–826.
[7] F. Wang, R. Deng, J. Wang, Q. Wang, Y. Han, H. Zhu, X. Chen, X. Liu, Nat. Mater. 10 (2011) 968–973.
[8] W. Zou, C. Visser, J. Maduro, M. Pshenichnikov, J. Hummelen, Nat. Photonics 6 (2012) 560–564.
[9] X. Xie, X. Liu, Nat. Mater. 11 (2012) 842–843.
[10] F. Zhang, S. Wong, ACS Nano 4 (2010) 99–112.
[11] F. Wang, X.G. Liu, Chem. Soc. Rev. 38 (2009) 976–989.
[12] G.F. Wang, Q. Peng, Y.D. Li, Acc. Chem. Res. 44 (2011) 322–332.
[13] F. Wang, X.G. Liu, J. Am. Chem. Soc. 130 (2008) 5642–5643.
[14] C.Y. Cao, H.K. Yang, J.W. Chung, B.K. Moon, B.C. Choi, J.H. Jeong, K.H. Kim, J. Mater. Chem. 21 (2011) 10342–10347.
[15] A.P. Alivisatos, Science 271 (1996) 933–937.
[16] M.A. El-Sayed, Acc. Chem. Res. 34 (2001) 257–264.
[17] R.N. Bhargava, D. Gallaghar, X. Hong, A. Nurmikko, Phys. Rev. Lett. 72 (1994) 416–419.
[18] H.X. Mai, Y.W. Zhang, R. Si, Z.G. Yan, L.D. Sun, L.P. You, C.H. Yan, J. Am. Chem. Soc. 128 (2006) 6426–6436.
[19] R.X. Yan, Y.D. Li, Adv. Funct. Mater. 15 (2005) 763–770.
[20] Y.P. Du, Y.W. Zhang, Z.G. Yan, L.D. Sun, S. Gao, C.H. Yan, Chem. Asian J. 2 (2007) 965–974.
[21] K.W. Krämer, D. Biner, G. Frei, H.U. Güdel, M.P. Hehlen, S.R. Lüthi, Chem. Mater. 16 (2004) 1244–1251.
[22] L. Wang, Y. Li, Nano Lett. 6 (2006) 1645–1649.
[23] Y. Yang, Y. Sun, T.Y. Cao, J.J. Peng, Y. Liu, Y.Q. Wu, W. Feng, Y.J. Zhang, F.Y. Li, Biomaterials 34 (2013) 774–783.
[24] Y. Li, G.F. Wang, K. Pan, W. Zhou, C. Wang, N.Y. Fan, Y.J. Chen, Q.M. Feng, B.B. Zhao, CrystEngComm 14 (2012) 5015–5020.
[25] R. Kumar, M. Nyk, T.Y. Ohulchanskyy, C.A. Flask, P.N. Prasad, Adv. Funct. Mater. 19 (2009) 853–859.
[26] M. Pollnau, D.R. Gamelin, S.R. Lüdel, Phys. Rev. B: Condens. Matter 61 (2000) 3337–3346.
[27] Y. Li, G.F. Wang, K. Pan, N.Y. Fan, S. Liu, L. Feng, RSC Adv. 3 (2013) 1683–1686.
[28] G.S. Qin, W.P. Qin, G.F. Wu, S.H. Huang, Solid State Commun. 125 (2003) 377–379.
[29] D. Zhao, W.P. Qin, J.S. Zhang, C.F. Wu, G.S. Qin, G. De, J.S. Zhang, S.Z. Lü, Chem. Phys. Lett. 403 (2005) 129–134.